Energy & Environmental Science

Accepted Manuscript

This is an *Accepted Manuscript*, which has been through the Royal Society of Chemistry peer review process and has been accepted for publication.

Accepted Manuscripts are published online shortly after acceptance, before technical editing, formatting and proof reading. Using this free service, authors can make their results available to the community, in citable form, before we publish the edited article. We will replace this *Accepted Manuscript* with the edited and formatted *Advance Article* as soon as it is available.

You can find more information about *Accepted Manuscripts* in the Information for Authors.

Please note that technical editing may introduce minor changes to the text and/or graphics, which may alter content. The journal's standard Terms & Conditions and the Ethical guidelines still apply. In no event shall the Royal Society of Chemistry be held responsible for any errors or omissions in this *Accepted Manuscript* or any consequences arising from the use of any information it contains.

ROYAL SOCIETY OF CHEMISTRY

www.rsc.org/ees

Energy & Environmetal Science

RSCPublishing

COMMUNICATION

$NaCrO_2$ cathode for high rate sodium-ion batteries

Cite this: *Energy Environ. Sci.*, 2015, xx, xxxx

Chan-Yeop Yu[a], Jae-Sang Park[a], Hun-Gi Jung[b], Kyung-Yoon Chung[b], Doron Aurbach[d,*], Yang-Kook Sun[c,*] and Seung-Taek Myung[a,*]

Received 00th January 2015,
Accepted 00th January 2015

DOI: 10.1039/x0xx00000x

www.rsc.org/ees

Sodium ion batteries offer a potential alternative or complementary system to lithium ion batteries, which are widely used in many applications. For this purpose, layered O3-type $NaCrO_2$ for use as a cathode material for sodium ion batteries was synthesized via an emulsion drying method. The produced $NaCrO_2$ was modified by pitch as a carbon source and the products were tested in half and full cells using a $NaPF_6$-based nonaqueous electrolyte solution. The carbon-coated $NaCrO_2$ cathode material exhibits excellent capacity retention with superior rate capability up to 150 C-rate (99 mAh (g-oxide)$^{-1}$), which corresponds to a full discharge during 27s. The surface conducting carbon layer plays a critically important role in the excellent performance of this cathode material. We confirmed the reaction process with sodium using X-ray diffraction and X-ray absorption spectroscopy. Thermal analysis using time-resolved X-ray diffraction also demonstrated the structural stability of the carbon-coated $Na_{0.5}CrO_2$. Due to the excellent performance of the cathode material described here, this work has the potential to promote accelerated development of sodium ion batteries for a large number of applications.

Introduction

Lithium ion batteries (LIB) have attracted a great deal of attention as an alternative energy power source to fossil fuels (in internal combustion engines) for ground transportation, due to their high energy density and good cyclability at moderate rates.[1-3] By virtue of these advantages, as the market of electric vehicles (EVs), portable devices and other devices using LIBs expands, the demand for large-scale energy storage devices is also gradually increasing. However, the percentage mass of lithium in the earth's crust is only 0.006%.[4] Indeed, the cost of lithium and lithium compounds may increase and Li sources may become depleted when EV use expands in the near future, which may cause a monopoly of the lithium resources. Also, we anticipate an increasing demand for large energy storage devices, in order to use more and more sustainable energy (e.g. from solar and wind sources). LIB will not be able to meet the demand for load leveling applications. For these reasons, many research groups throughout the world are trying to address this problem by developing new sodium ion batteries (SIB) as a substitute or complementary systems for LIB. Sodium, an abundant element (Clarke's number is 2.64[4]), and sodium compounds offer an alternative to the expensive and less abundant lithium and Li compounds in batteries, due to the low redox potential of sodium and the capability of sodiated transition metal oxides to serve as effective sodium intercalation electrode materials.[5,6] Competitive cost, cyclability, and rate capability are necessary for the use of SIBs in large-scale energy storage systems.[6] Hence, there is a strong incentive to explore and develop effective and novel SIB systems.

Recently, several groups have investigated layer-structured sodium intercalation compounds for the application of low-cost and large-scale energy storage.[7-22] In 1982, Hagenmuller *et al.*[23] confirmed the feasibility of using $NaCrO_2$ as a Na^+ extraction/insertion electrode. Recently, Komaba's group[7] revisited O3-type layer-structured $NaCrO_2$ in which Na ions could be inserted into/extracted from the host structure due to its larger inter-slab distance compared to $LiCrO_2$ material, which is electrochemically inactive in Li-based electrolyte solutions.[24] Furthermore, certain remarkable advantages of $NaCrO_2$ have been reported, including a high theoretical capacity of about 250 mAh g^{-1} although the practical reversible capacity is approximately 110 mAh g^{-1} ($Na_{1-x}CrO_2$, $0 \le x \le 0.5$), of which the voltage profile flattens at 3 V. Dahn's group[8] also reported that desodiated $Na_{0.5}CrO_2$ has good thermal stability in

Energy & Environmental Science Accepted Manuscript

Na-based nonaqueous electrolytes. A citric acid-assisted carbon coating also showed a slight improvement in the cycling stability of $NaCrO_2$ electrodes but was not successful for achieving high rate capability.[9] Summarizing these reports, we can simply state that the $NaCrO_2$ electrodes described there delivered an initial discharge capacity of about 100 – 110 mAh g^{-1} supported by $Cr^{3+/4+}$ redox activity via O3 to P3 phase transition, exhibited fast capacity fading (*ca*. 80% at 50th cycle) and a disappointing rate capability. Although the thermal stability reported was relatively good, the overall impression from all the previous work on $NaCrO_2$ was not very encouraging.

Despite this, we decided to attempt to improve this cathode material by applying new synthetic routes. Our approach led to $NaCrO_2$ cathodes with excellent capacity retention, impressive rate capability and feasibility in full cells suitable for advanced energy storage and conversion. In order to overcome the above-mentioned drawbacks, we synthesized $NaCrO_2$ via a water-in-oil type emulsion drying method, which can intermix cations homogeneously at the atomic level, and then subsequently modified the surfaces of the products using pitch (scheme 1). This pioneering work led to $NaCrO_2$ cathodes of unprecedented high performance, achieved by optimizing the synthetic methods including surface modification with electro-conducting carbon, which enabled a great improvement in the electric conductivity to 0.47 S cm^{-1} from 8 x 10^{-5} S cm^{-1} for the bare $NaCrO_2$. Before the work described in this paper, nobody had attempted to synthesize $NaCrO_2$ by methods other than the solid-state approach or had suggested the possibility of demonstrating full sodium ion batteries based on $NaCrO_2$ (hereafter referred as to be C-$NaCrO_2$) cathodes coupled with hard carbon anodes. Our work allows us to state with a high degree of confidence that the carbon-coated $NaCrO_2$ cathode is eminently suitable for use in high-rate Na-ion batteries for energy storage applications.

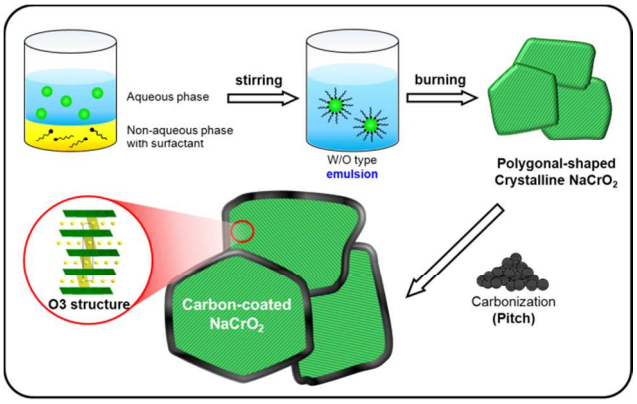

Scheme1 Synthesis of C-$NaCrO_2$ via the novel emulsion method.

Results and discussion

As shown in Scheme 1, the preparation of the emulsion may produce oily particles in water. Though an emulsion is easily separated into water and oil phases, the addition of an emulsifying agent prevents this separation, stabilizing the emulsion. Heating the oily precipitates at 400^{o}C in air almost completely removes the organic components contained in the emulsion, resulting in solid powders that exhibit low crystallinity, although the product is crystallized into an O3-type layer structure (Fig. S1). The crystallinity improves with increasing calcination temperature in an Ar atmosphere. As a result, highly crystalline $NaCrO_2$, which has an olive-green color (inset of Fig. 1a), is produced through calcination at 900^{o}C for 10 h in Ar (Fig. 1a). Rietveld refinement of the XRD data was carried out assuming a rhombohedral $R\bar{3}m$ space group, excluding the possibility of site exchange between Na^+ and Cr^{3+} due to the great difference in their ionic radii. The observed pattern is almost identical to that of the simulated pattern, indicating that the material was well synthesized (Fig. 1a) with R_{wp} value of 11.1%. The TEM image demonstrates that the emulsion-derived $NaCrO_2$ exhibits hexagonal plate-like particles with smoothly developed edges (Fig. 1b).

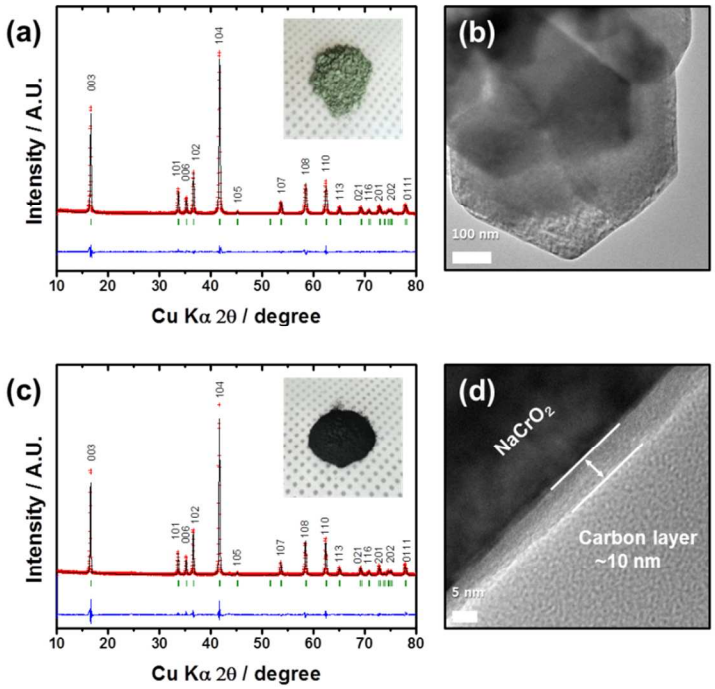

Fig.1 (a) Rietveld refinement of the XRD patterns of the bare $NaCrO_2$ powders. (b) TEM image of polygonal-shaped bare $NaCrO_2$ particles. (c) Rietveld refinement of the XRD patterns of the C-$NaCrO_2$ powders. (d) TEM image of C-$NaCrO_2$ and carbon layer below 10 nm. Photographs are also shown in the insets

contained approximately 3.4 wt. % of carbon residue analysed by CHN analyser, was also a highly crystalline black-colored product (Fig. 1c). There are no significant changes in the particle morphology of $NaCrO_2$ before and after the carbon coating except a change in colour (Fig. S2). Rietveld refinement of the XRD pattern indicates that the carbon coating did not alter the crystal structure as there were no changes of the peak intensity and impurities, as further confirmed by the lattice parameter results (Table S1). Further increase in the carbon content did not lower the peak intensity (Fig. S3), and the resulting lattice parameters remained constant for all the samples (Table S1). The TEM image clearly shows the presence of a foreign layer, carbon, on the surface of $NaCrO_2$

Energy & Environmental Science Accepted Manuscript

This journal is © The Royal Society of Chemistry 2012

(Fig. 1d). Increasing the carbon content resulted in gradual growth of the carbon layers to approximately 30 nm (Figs. S3).

The Raman spectrum of this material provides further evidence that the carbon layers reside on the surface of the $NaCrO_2$ particles (Fig. 2a). Only the background is observed for the bare $NaCrO_2$ due to the absence of carbon on the compound. By contrast, the D-band and G-band, indicating clear evidence of carbon, appeared at 1,350 and 1,600 cm^{-1}, respectively, in the C-$NaCrO_2$. In particular, the intense G-band peak relative to the broad D-band means that the carbon layer is quite crystallized due to the carbonization of pitch in the Ar atmosphere. As a result, the presence of a crystallized carbon coating dramatically improved the electric conductivity of $NaCrO_2$, although the residue is small, 1.4 wt. % (4.4×10^{-3} S cm^{-1}), after which the conductivity increased almost linearly to 4.7×10^{-1} S cm^{-1} (14.6 wt. %) with increasing carbon content (Fig. 2b).

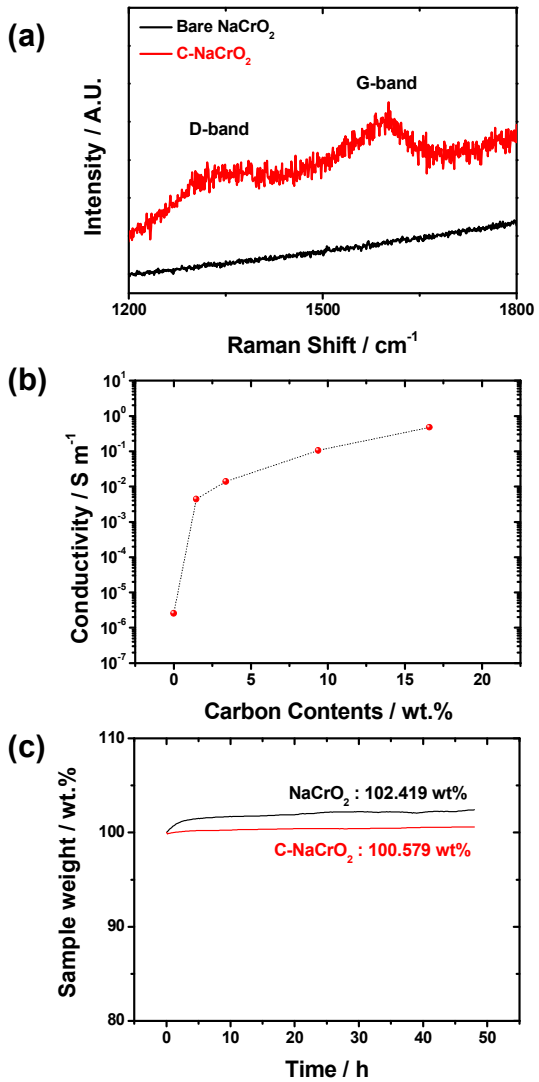

Fig. 2 (a) Raman spectroscopy of the bare and C-$NaCrO_2$, (b) electric conductivity of $NaCrO_2$ as a function of the carbon content, and (c) TG data of $NaCrO_2$ obtained in ambient air for 50 h.

A serious problem of sodiated cathode materials is immediate water absorption, which occurs within 2 h after exposure to ambient air. This then leads to the formation of NaOH and Na_2CO_3 on the surface of bare $NaCrO_2$ (Fig. S4 a and b), as evidenced by the weight increase measured by TGA (Fig. 2c) and ToF-SIMS (Fig. S4b). Since the sodium diffuses to the surface, electrochemically inactive parts are formed inside the particles. Even more seriously, the formed NaOH and Na_2CO_3 are electrical insulators and this, in turn, increases the resistance of the active mass. Unexpectedly, we discovered that the carbon coating layer suppresses moisture uptake due to its hydrophobic characteristics. Therefore, the crystal structure does not change even after air exposure for 48 h, while the bare $NaCrO_2$ undergoes phase separation into Na-deficient Na_xCrO_2 and NaOH (Fig. S4a) after even brief exposure to air.

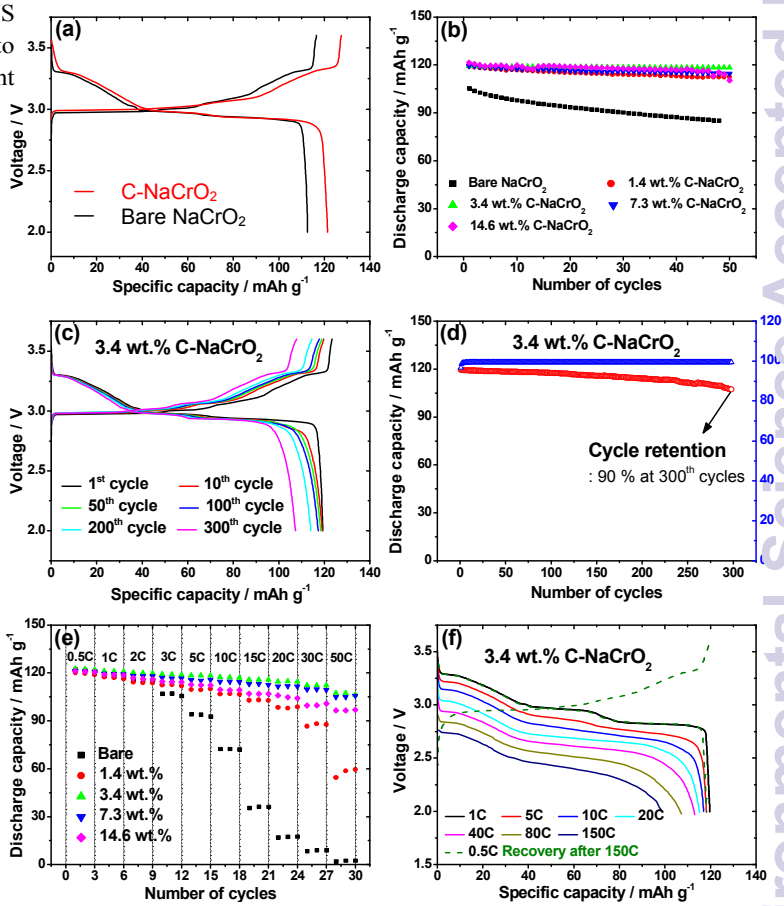

Fig. 3 Electrochemical performances of bare and C-$NaCrO_2$ using Na metal as the counter electrode and 0.5 M $NaPF_6$ PC:FEC solvent as the electrolyte: (a) first charge and discharge curves. Cells were tested in the voltage range of 2.0 to 3.6 V at a current density of 20 mA g^{-1}. (b) Cycle plots as a function of the amount of contained carbon. (c) Charge and discharge curves and (d) cycle performance up to 300 cycles of the 3.4 wt.% carbon-coated electrode. (e) Rate capability as a function of the amount of contained carbon. (f) Rate performances of the 3.4 wt. % C-$NaCrO_2$, which showed the best results among the various carbon contents.

The electrochemical performances of bare and C-$NaCrO_2$ were measured by applying a constant current density of 20 mA g^{-1} in the voltage range of 2.0 to 3.6 V at 25°C. The first charge-discharge curves of the bare and the C-$NaCrO_2$ (3.4 wt. %) are identical to each other except for the capacity, which is 112 mAh g^{-1} and 121 mAh g^{-1}, respectively, on discharge (Fig. 3a). It is obvious that the carbon coating enables more capacity

Energy & Environmental Science Accepted Manuscript

delivery above 3.07 V on charging, which seems to be related to the phase transformation from an O3 to P3 layer structure, as mentioned below, and is reversible upon discharge. Despite the severe capacity fading observed for the bare $NaCrO_2$, the C-$NaCrO_2$ electrodes displayed excellent cycle performance, above 96% capacity retention after the 50th cycle for the carbon-coated electrodes with carbon contents of 1.4–14.2 wt.%. In particular, the 3.4 wt.% C-$NaCrO_2$ electrode, which exhibited the best performance among the electrodes (Fig. 3b), had a surprising capacity retention upon cycling of approximately 90% at the 300th cycle (Figs. 3c and d), showing a coulombic efficiency approaching 100 % apart from the first cycle. The rate performance results for the C-$NaCrO_2$ electrodes were surprising (Figs. 3e and f). The delivered capacity was only 3 mAh g^{-1} for the bare $NaCrO_2$ at 50 C-rate. By contrast, the 3.4 and 7.3 wt.% C-$NaCrO_2$ electrodes delivered unexpectedly high capacities (106 mAh g^{-1}) at 50 C-rate (5.5 A g^{-1}), retaining 87% of the capacity obtained at 0.5 C-rate (55 mA g^{-1}). The superior rate capacity was further evidenced up to 150 C-rate (16.5 A g^{-1}), which corresponds to a 27s discharge (Fig. 3f), in which the delivered capacity (99 mAh g^{-1}) is solely associated with the Na^+ insertion reaction as is obvious from the flat discharge curve. The original capacity (119 mAh g^{-1} at 0.5 C-rate) was easily recovered after any operation at high rates. It is most likely that this excellent rate property is due to the presence of crystalline carbon layers, assisting the immediate migration of electrons so that the sodium ions can be inserted or extracted at ultrafast rates. Residual carbon content was also equalized for both bare and C-$NaCrO_2$ to observe the effect of carbon coating (Fig. S6). However, the resulting electrochemical performance was disappointing for the bare $NaCrO_2$. A previous report by Ding et al.[9] suggests that a citric-acid derived carbon coating improves the cycling stability. In our results, the carbon coating contributes not only to the cycling performance, but also to a very high rate performance, which has not been reported previously. In order to enhance stability of the cells, we tested the solutions contained FEC as an important active additive that improves electrodes passivation. We proved that the excellent performance of this cathode material is intrinsic and does not relate to the solution used. Its excellent rate capability was demonstrated also in FEC free solutions (Fig. S7).

The electrode structures were investigated using *ex situ* XRD in order to clarify the mechanism of the charge and discharge processes. Fig. 4a shows the voltage profile of the first cycle for the C-$NaCrO_2$ (3.4 wt. %) plotted as a function of the Na^+ content, δ, in $Na_{1-\delta}CrO_2$. As anticipated, the phase transition from O3 to the other phases is evident from the data. The original hexagonal O3 phase ($NaCrO_2$; S.G. = $R\bar{3}m$, JCPDS card #88-0720) is maintained with δ = 0.17 in $Na_{1-\delta}CrO_2$ (Fig. 4b), after which the monoclinic O3 phase ($Na_{0.74}CrO_2$; S.G. = *C2/m*, JCPDS card #38-1204) appears at δ = 0.42 in $Na_{1-\delta}CrO_2$, accompanied by the formation of new 2θ peaks at 32.7°, 35.7°, 36.7° and overlapped 42.1°. From δ = 0.33 in $Na_{1-\delta}CrO_2$, the newly formed monoclinic P3 phase ($Na_{0.52}CrO_2$; S.G. = *R3m*, JCPDS card #38-1205) is dominant until the end of charge. The difference in the capacity of about 10 mAh g^{-1} above 3.07 V belongs to the region of phase transformation from monoclinic O3 to monoclinic P3. It seems that the phase transformation takes place more readily for the carbon-coated $NaCrO_2$, probably due to the high electrical conductivity, such that a higher capacity can be delivered. This series of phase transitions occurs based on the gliding mechanism of the transition metal layer slab suggested by Delmas *et al.*[25] Chemical diffusion of Na^+ at the end of charging for $Na_{0.5}CrO_2$ with the monoclinic P3 structure (~10^{-9} S cm^{-1}) is much faster than that of $Na_{0.92}CrO_2$ with hexagonal O3 (~10^{-13} S cm^{-1}) due to the large interlayer distance. From these results, we confirmed that the phase transition progresses in a sequence of hexagonal O3 → monoclinic O3 → monoclinic P3 on charge and *vice versa* on discharge, which coincides with prior results in the literature.[10,20,26]

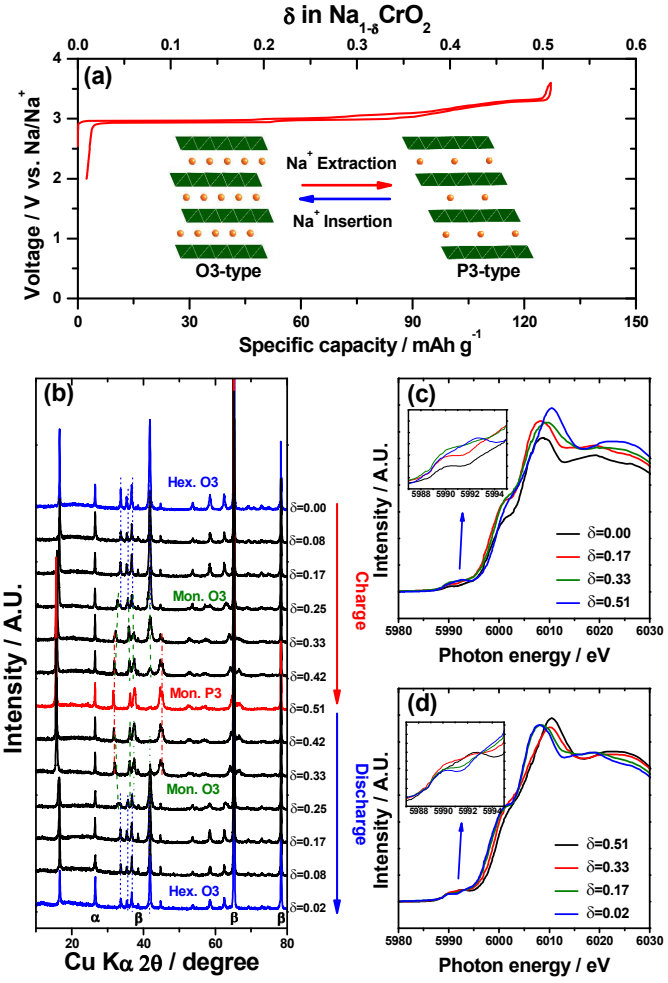

Fig. 4 $NaCrO_2$ during the insertion/extraction of sodium ions. (a) First charge and discharge curve along with a schematic of the phase transition. (b) *Ex situ* XRD patterns obtained during charge and discharge. The impurity peaks of α and β are graphite and Al foil, respectively. Cr K-edge XANES spectra obtained during (c) charge and (d) discharge.

Energy & Environmental Science Accepted Manuscript

This journal is © The Royal Society of Chemistry 2012

Cr K-edge XANES was employed to monitor the change in the oxidation states during charge and discharge. In the charge process (Fig. 4c), the white line peak shows a positive shift to a higher energy as the extent of de-sodiation increases. Moreover, the pre-edge peak at 5,990 eV gradually broadens with desodiation and finally splits into two broad peaks (5,990 eV and 5,992 eV) at the end of charge, $\delta = 0.51$ in $Na_{1-\delta}CrO_2$. This is due to the 1s to 3d transition characteristics of Cr oxidation. Therefore, the observed increase in the pre-edge peak at 5,992 eV indicates the oxidation of Cr, presumably to Cr^{4+}. Further increase in the peak at 5,992 eV indicates the formation of Cr^{6+}. However, this behaviour was not observed in the present study. During discharge, the chemical shift returns toward the lower energy side with a relative decrease of the pre-edge peak (Fig. 4d), indicating that the oxidized Cr is reduced to Cr^{3+}. The variation in the oxidation state is highly reversible and the unit cell parameters also recover to nearly the same value as the pristine carbon-coated $NaCrO_2$. Therefore, it can be concluded that the $Cr^{3+/4+}$ redox couple is reversibly available, since $NaCrO_2$ delivers a reversible capacity of approximately 121 mAh g^{-1} with excellent cyclability (90% for 300 cycles, Figs. 3c and d).

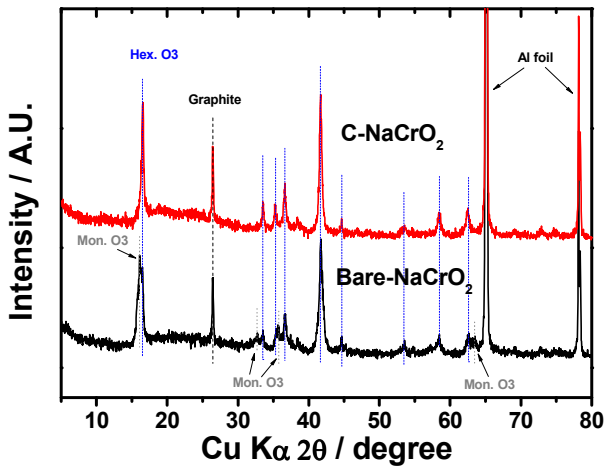

Fig. 5 *Ex situ* XRD patterns of bare electrode after 50 cycles (bottom) and C-$NaCrO_2$ electrode after 300 cycles (top)

The structural stabilities of both the bare and C-$NaCrO_2$ electrodes were examined by XRD after extensive cycle tests (Fig. 5). For bare $NaCrO_2$, the resulting XRD pattern shows broadening of the diffraction peaks due to the coexistence of hexagonal O3 $NaCrO_2$ with a monoclinic O3 phase, which is the intermediate product appearing in the range of $\delta = 0.25$–0.42 in $Na_{1-\delta}CrO_2$ (Fig. 4b). The differentiation curves suggest gradual capacity fading in the voltage plateau of 2.94–2.99 V upon discharge, in particular, where the region is dominant with the monoclinic O3 structure (Fig. S5). Hence, the poor cycling performance can be understood (Fig. 2b). Meanwhile, the phase recovery to hexagonal O3 seems to occur smoothly, such that the original hexagonal O3 structure is maintained up to the 300th cycle for the C-$NaCrO_2$. It is interesting that the only difference between the two types of electrodes is the presence of a carbon coating layer. We assume that the series of phase transformation may induce stress in the oxide lattice because the large Na^+ ions (1.02Å) diffuse in and out of the structure. Nevertheless, the highly electro-conducting, crystalline carbon layer on the Na_xCrO_2 particles renders a facile migration of Na^+ ions in the structure, which is confirmed by a complete recovery of the original structure of the active mass even after 300th cycles. This is well expressed by the excellent capacity retention of this cathode material (90% for 300 cycles, Figs. 3c and d). The highly conductive surface of the particles facilitates Na^+ extraction and insertion, promoting a fast electron transfer to the $Cr^{3+/4+}$ redox couple.

Full sodium ion cells using $NaCrO_2$ as the cathode material and hard carbon as the anode material were fabricated (pouch cell configuration), as illustrated in Fig. 6a. After the cell formation process, the initial charge and discharge profiles of cells containing bare and C-$NaCrO_2$ were compared in the voltage range of 1.8–3.4 V. The initial capacities were approximately 97 and 102 mA h g^{-1} for the bare and C-$NaCrO_2$

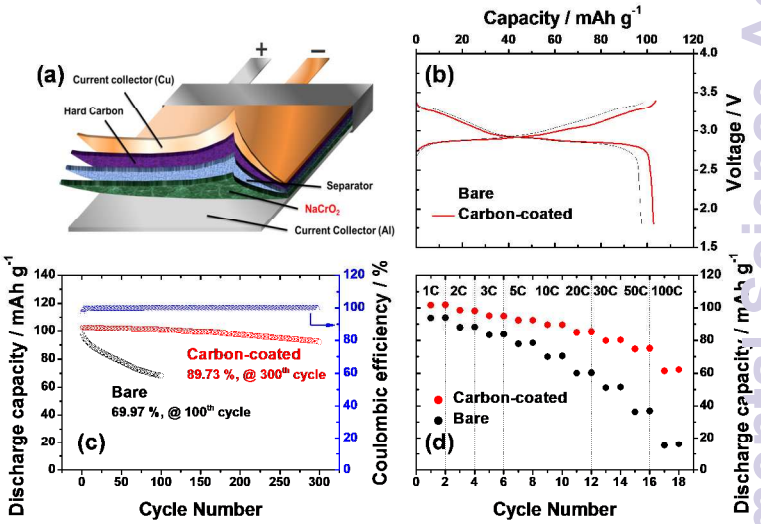

Fig. 6 (a) Illustration of $NaCrO_2$||0.5 M $NaPF_6$ in PC:FEC||Hard carbon full sodium ion battery. (b) First charge and discharge cycles of bare and C-$NaCrO_2$ at 20 mA g^{-1} from 1.8 to 3.4 V at 25°C. (c) Cycle performance of the $NaCrO_2$ full cell. (d) Rate capability at various C-rates.

cathodes, respectively. Cycling performance and rate capability of cells with bare $NaCrO_2$ cathodes were disappointing (70% at the 100th cycle). By contrast, the capacity retention of cells with C-$NaCrO_2$ cathodes was approximately 90% after 300 cycles, showing a coulombic efficiency approaching 100 %. Also, a superior rate capability was observed even at 100 C-rate (10 A g^{-1}) for the full cells containing C-$NaCrO_2$ cathodes (Fig. 6d and Fig. S8). We compared the electrochemical properties of several O3- and P2-type layered cathode materials to confirm the novelty of the C-$NaCrO_2$ cathodes developed in the present work (Table S2). This comparison demonstrates the competitiveness of the C-$NaCrO_2$ material in terms of capacity retention during prolonged cycling and high rate capability,

Energy & Environmental Science Accepted Manuscript

which have not been achieved previously in rechargeable Na battery systems. These data indicate that the $Cr^{3+/4+}$ redox reaction can be successfully utilized leading to high performance of O3-type layer compounds when coated by appropriate electro-conducting carbon layers.

Thermal stability is another important parameter that should be investigated before these electrode materials are considered for use in practical power sources. A combination of thermo-gravimetric analysis (TGA) and *in situ* high-temperature XRD (HT-XRD) provided important information on the thermal behaviour of these cathode materials. The TGA and HT-XRD studies help to better interpret the more complicated differential scanning calorimetric (DSC) measurements. For the thermal studies, cathodes comprising coated and bare $NaCrO_2$ were electrochemically desodiated to form $Na_{0.5}CrO_2$. The observed weight loss in TGA measurements, which is mainly ascribed to oxygen evolution from the parent oxide, varied among the samples (Fig. 7a). The bare $Na_{0.5}CrO_2$ exhibits progressive weight loss followed by three steps up to 400°C: the first step from 25°C to 140°C (0.9 wt. % loss), the second step from 140°C to 280°C showing a violent weight loss (3.9 wt. %), and the third step from 280°C to 400°C (3.3 wt. %). From the HT-XRD measurements it is clear that the distorted monoclinic P3 phase, $Na_{0.5}CrO_2$, is stable up to 140°C, which belongs to the first step with a weight loss of 0.9 wt. % (Figs. 7a and c). As oxygen is further evolved from the parent structure to 280°C, the monoclinic P3 phase is relaxed to a hexagonal P3 phase at 150°C, showing that the $(201)_{Mon.}$ and $(11\text{-}2)_{Mon.}$ peaks at 45° (2θ) merge to the $(105)_{Hex.}$ peak in the second step. The hexagonal P3 phase is maintained as a single phase up to 280°C. Above this temperature, a new P3 phase with a short interlayer distance appears and was found to be P3 CrO_2.[8] The CrO_2 phase develops further as the temperature is increased even more. Interestingly, a hexagonal O3 $NaCrO_2$ phase also appears as the P3 CrO_2 appears above 290°C for the bare Na_xCrO_2 material. As a result, the heating of desodiated $Na_{0.5}CrO_2$ induces oxygen evolution from the oxide lattice and this simultaneously results in the phase segregation of $Na_{0.5}CrO_2$ and CrO_2.

By contrast, the variation in weight for the C-$Na_{0.5}CrO_2$ (Fig. 7b) is significantly lower, and takes place in three steps: the first step from 25°C to 170°C (0.4 wt. % loss), the second step from 170°C to 320°C showing a gradual weight loss (1.3 wt. %), and the third step from 320°C to 400°C (1.2 wt. %). The phase transition from monoclinic P3 to hexagonal P3 is delayed to 170°C, after which the hexagonal phase is predominantly present in the temperature range of 170–320°C (Fig. 7b and c). Above 320°C, the appearance of P3 CrO_2 can be seen, while that of O3 hexagonal $NaCrO_2$ is not observed in the XRD pattern up to 400°C. However, the diffraction intensity is low and broad for the P3 CrO_2 formed by the thermal treatment of C-$Na_{0.5}CrO_2$ (Fig. 7c) compared to behaviour of the bare cathode material. On comparing the oxygen evolution for both samples, we found that the C-$Na_{0.5}CrO_2$ showed a weight loss of only 2.9 wt. % up to 400°C, which is lower than that of bare $Na_{0.5}CrO_2$ (8.1 wt. %). The lower evolution of oxygen from the crystal structure is likely to retard the phase segregation. Another interesting feature is that the desodiated $Na_{0.5}CrO_2$ does not produce a cubic spinel phase, as formed by delithiated transition metal oxides[27], even after oxygen release from the parent oxide.

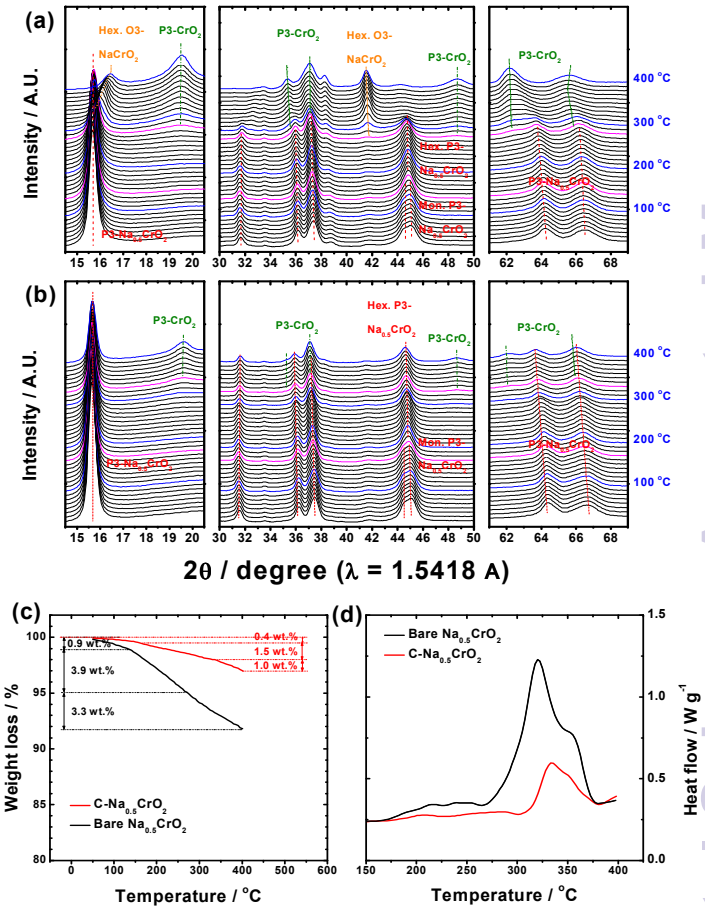

Fig. 7 (a) TR-XRD patterns of electrochemically desodiated (a) bare $Na_{0.5}CrO_2$ and (b) C-$Na_{0.5}CrO_2$. (c) TG results of bare and C-$Na_{0.5}CrO_2$. (d) DSC results of bare and C-$Na_{0.5}CrO_2$.

Based on these experimental results, the DSC behaviour of these electrodes can be understood (Fig. 7d). For the bare sample, the small heat evolution in the temperature range of 150–270°C is due to the phase transition from monoclinic P3 to a hexagonal P3 phase. As oxygen is further evolved from the crystal structure, the hexagonal P3 phase undergoes phase segregation with Na-rich $Na_{0.5}CrO_2$ and Na-deficient CrO_2 accompanying the exothermic reaction in the temperature range of 270–360°C. For the C-$Na_{0.5}CrO_2$, phase transformation takes places over a wide temperature range of 170–320°C. In addition, the observed exothermic heat induced from the phase separation process is also greatly reduced because of the slow oxygen evolution from the crystal structure. The difference of the oxygen content could be related to the degree of heat generated during the exothermic reaction. Even after the exothermic reaction is complete, the weight loss is smaller for the C-$Na_{0.5}CrO_2$ material up to 400°C. This is attributed to the

Energy & Environmental Science Accepted Manuscript

This journal is © The Royal Society of Chemistry 2012

presence of the carbon coating layer on the surface of the $Na_{0.5}CrO_2$ particles, which prevents thermal damage to the crystal structure. Therefore, it is evident that the carbon coating retards the exothermic decomposition reaction at higher temperatures with less heat generation (scheme 2).

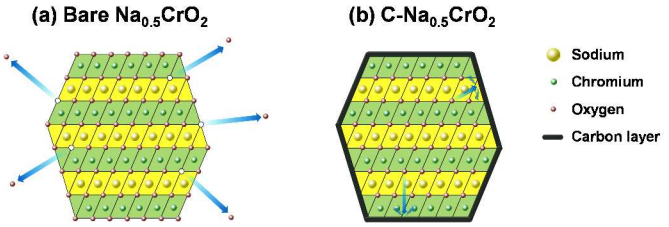

Scheme 2 Thermal mechanism of de-sodiated $Na_{0.5}CrO_2$ at high temperature.

Conclusion

Layered O3-type $NaCrO_2$ was successfully synthesized by an emulsion drying method, which seems to be a better synthetic route than previously reported syntheses of such materials. The surfaces of the $NaCrO_2$ particles were modified by carbon to impart them with a high electrical conductivity of approximately 10^{-1} S cm^{-1}. C-$NaCrO_2$ cathodes exhibited excellent cyclability and an ultrafast rate capability up to a 150 C-rate. It is clear that the high electrical conductivity successfully promotes the reversible insertion and extraction of sodium ions, accompanied by a facile complementary red-ox reaction of the Cr^{4+}/Cr^{3+} couple. Excellent electrochemical performance of these cathodes was demonstrated in both half and full sodium ion cells. In addition, the heat generation of de-sodiated C-Na_xCrO_2 is relatively small due to the suppression of oxygen evolution during the exothermic reaction resulting from the presence of the carbon coating layer. All of these findings demonstrate the potential importance of C-$NaCrO_2$ cathodes for advanced sodium ion batteries for many applications, including large-scale energy storage devices.

Experimental

$NaCrO_2$ powders were synthesized by the emulsion drying method (Scheme 1). The starting materials used for the synthesis of $NaCrO_2$ were sodium nitrate ($NaNO_3$) and chromium nitrate nonahydrate ($Cr(NO_3)_3{\cdot}9H_2O$) using kerosene as an oil solution and Tween #85 as a surfactant. The preparation of the emulsion and the emulsion drying process have been described in our prior work.[28,29] The obtained powders were preliminary annealed at 400°C for 4 h in air and then calcined at 900°C for 10 h in an Ar atmosphere. The produced $NaCrO_2$ powders were rapidly moved into an Ar-filled glove box to avoid contamination with moisture, which causes the formation of NaOH on the surface of $NaCrO_2$. As-synthesized $NaCrO_2$ powders were mixed with an appropriate amount of pitch, 1–20 wt. % versus $NaCrO_2$, as a carbon source to produce C-$NaCrO_2$ by heating at 750°C for 5 hours in an Ar atmosphere.

Phase identification of the calcined products was obtained by X-ray diffraction (XRD, Rint-2000, Rigaku) using Cu Kα radiation. The XRD data were obtained with a step size of 0.03° and a count time of 3s. The presence of carbon was observed by transmission electron microscopy (TEM, JEM-3010, JEOL) and Raman spectroscopy (Renishaw, InVia Raman microscope). The DC electrical conductivity was measured by a direct volt-ampere method (CMT-SR1000, AIT), in which disc samples were contacted with a four-point probe. An elemental analyzer (EA110, CE Instrument, Italy) was employed to determine the amount of carbon in the final products. The XAS measurements were performed on the 1D beamline in the 2.5 GeV Pohang Light Source (ring current of 120−160 mA), which is a third-generation synchrotron radiation source. The Cr K-edge XAS data were obtained in the total electron yield mode and the sample current was recorded. Ion chamber detectors filled with high purity N_2 were used to record the X-ray absorption spectra. The electrochemically delithiated powders were subjected to TGA (loaded sample amount: 10 mg, DTG-60, SHIMADZU, Japan). The thermal properties were analyzed up to 400°C by time-resolved XRD (TR-XRD, R-AXIS IV++, Rigaku). The obtained powder samples were sealed completely and mounted on the thermal stage of the TR-XRD system. Mo-Ka radiation with a wavelength of 0.7107 Å, which was converted to the value of the Cu-Ka wavelength (1.5418 Å) for convenience, was used in the X-ray diffractometry system at KIST.

For electrode fabrication, the synthesized bare $NaCrO_2$ and carbon-coated samples were separately mixed with KS-6 and Super-P (1:1 in weight) as conducting materials and polyvinylidene fluoride (85:7.5:7.5 in weight) in *N*-methylpyrrolidon (NMP). The obtained slurry was coated onto Al foils and roll-pressed. The electrodes were vacuum-dried overnight at 110°C prior to use. The typical amount of loaded active material was approximately 3.5 mg cm^{-2}. Charge-discharge tests were performed using R2032 type coin cells for the half cell (Na metal anode) and the pouch-type full cells (hard carbon anode). Galvanostatic electrochemical charge and discharge tests were carried out in a 0.5M $NaPF_6$ in PC:FEC[30] (98:2 v/v mixture) solutions at room temperature. The presence of small amount of FEC in PC solutions was important for maintaining very good electrode passivation.[30]

Acknowledgements

This work was supported by the Human Resources Development program (No. 20124010203310) of the Korea Institute of Energy Technology Evaluation and Planning (KETEP) grant funded by the Korea government Ministry of Trade, Industry and Energy. This research was also supported by Basic Science Research Program through the National Research Foundation of Korea (NRF) funded by the Ministry of Education, Science and Technology of Korea (NRF-2014R1A2A1A11051197).

Notes and references

Energy & Environmental Science Accepted Manuscript

[a]*Department of Nano Science and Technology, Sejong University 98 Gunja-dong, Gwangjin-gu, Seoul, 143-747, South Korea. E-mail: smyung@sejong.ac.kr*
[b]*Center for Energy Convergence, Korea Institute of Science and Technology, Seoul 136-791, South Korea*
[c]*Department of Energy Engineering, Hanyang university, Seoul 133-791, South Korea. E-mail: yksun@hanyang.ac.kr*
[d]*Department of Chemistry, Bar Ilan University, Ramat-Gan, 52900, Israel. E-mail: Doron.Aurbach@biu.ac.il*

† Electronic Supplementary Information (ESI) available: [details of any supplementary information available should be included here]. See DOI: 10.1039/c000000x/

1 Y.K. Sun, Z. Chen, H.J. Noh, D.J. Lee, H.G. Jung, Y. Ren, S.Wang, C.S. Yoon5, S.T. Myung and K. Amine, Nature Mater., 2012, **11**, 942
2 H.G. Kim, S.T. Myung, J.K. Lee, Y.K. Sun, J. Power Sources, 2011, **196**, 6710
3 S.T. Myung, K.S. Lee, Y.K. Sun, H. Yashiroa, J. Power Sources, 2011, **196**, 7039
4 D.R. Lide, CRC Handbook of Chemistry and Physics, 86 edn., 2005, Section 4, 4-1
5 V. Palomares, P. Serras, I. Villaluenga, K.B. Hueso, J. Carretero-González, T, Rojo, Energy Environ. Sci., 2012, **5**, 5884
6 B.L. Ellis, L.F. Nazar, Curr. Opin. Solid State Mat. Sci., 2012, **16**, 168
7 S. Komaba, C. Takei, T. Nakayama, A. Ogata, N. Yabuuchi, Electrochem. Commun., 2010, **12**, 355
8 X. Xia, J.R Dahn, Electrochem. Solid-State Lett., 2012, **15**, A1
9 J.J. Ding, Y. Zhou, Q. Sun, Z. Fu, Electrochem. Commun., 2012, **22**, 85
10 S. Komaba, T. Nakayama, A. Ogata, T. Shimizu, C. Takei, S. Takada, A. Hokura, I. Nakai, ECS Trans., 2009, **16**, 43
11 C. Delmas, J. Braconnier, C. Fouassier, P. Hagenmuller, Solid State Ion., 1981, **3**, 165
12 X. Ma, H. Chen, G. Ceder, J. Electrochem. Soc., 2011, **158**, A1307
13 A. Caballero, L. Hernan, J. Morales, L. Sanchez, J. Santo Pena, and M.A.G. Aranda, J. Mater. Chem., 2012, **12**, 1142
14 D. Hamani, M. Ati, J.M. Tarascon, and P. Rozier, Electrochem. Commun., 2011, **13**, 938
15 S. Komaba, N. Yabuuchi, T. NaKayama, A. Ogata, T. Ishikawa, and I. Nakai, Inorg. Chem., 2012, **51**, 6211
16 N. Yabuuchi, M. Kajiyama, J. Iwatate, H. Nishikawa, S. Hitomi, R. Okuyama, R. Usui, Y. Yamada, and S. Komaba, Nature Mater., 2012, **11**, 512
17 S.M. Oh, S.T. Myung, C.S. Yoon, J. Lu, J. Hassoun, B. Scrosati, K. Amine, and Y.K. Sun, Nano Lett., 2014, **4**, 1620
18 D. Kim, E. Lee, M. Slater, W. Lu, S. Rood, and L.S. Johnson, Electrochem. Commun., 2012, **18**, 66
19 M. Sathiya, K. Hemalatha, K. Ramesha, J.M. Tarascon, and A.S. Prakash, Chem. Mat., 2012, **24**, 1846
20 Y.N. Zhou, J.J. Ding, K.W. Nam, X. Yu, S.M. Bak, E. Hu, J. Liu, J. Bai, H. Li, Z.W. Fu and X.Q. Yang, J. Mater. Chem. A, 2013, **1**, 11130
21 H. He, G. Jin, H. Wang, X. Huang, Z. Chen, D. Sun, Y. Tang, J. Mater. Chem. A, 2014, **2**, 3563
22 H. He, Z. Zeng, H. Wang, N. Chen, D. Sun, Y. Tang, Z. Huang, Y. Pan, J. Electrochem. Soc., 2015, **162**, A39.
23 J. J. Braconnier, C. Delmas, P. Hagenmuller, Mat. Res. Bull, 1982, 17, 993
24 S.T. Myung, S. Komaba, N. Hirosaki, N. Kumagai, Electrochem. Commun., 2002, **4**, 397
25 F. Tournadre, L. Croguennec, I. Saadoune, D. Carlier, Y. Shao-Horn, P. Willmann, and C. Delmas, J. Solid State Chem., 2004, **177**, 2790
26 K. Kubota, I. Ikeuchi, T. Namakaya, C. Takei, N. Yabuuchi, H. Shiiba, M. Nakayama, S. Komaba, J. Phy. Chem. C, 2015, **119**, 166
27 S.T. Myung, K.S. Lee, C.S. Yoon, Y.K. Sun, K. Amine, and Hitoshi Yashiro, J. Phys. Chem. C, 2010, **114**, 4710
28 S.T. Myung, H.-T. Chung, J. Power Sources, 1999, **84**, 32
29 S.T. Myung, N. Kumagai, S. Komaba, H.-T. Chung, J. Appl. Electrochem., 2000, **30**, 1081
30 S. Komaba, T. Ishikawa, N. Yabuuchi, W. Murata, A. Ito, Y. Ohsawa, ACS Appl. Mater. Interfaces, 2011, **3**, 4165

Energy & Environmental Science Accepted Manuscript

 This journal is © The Royal Society of Chemistry 2012

TOC

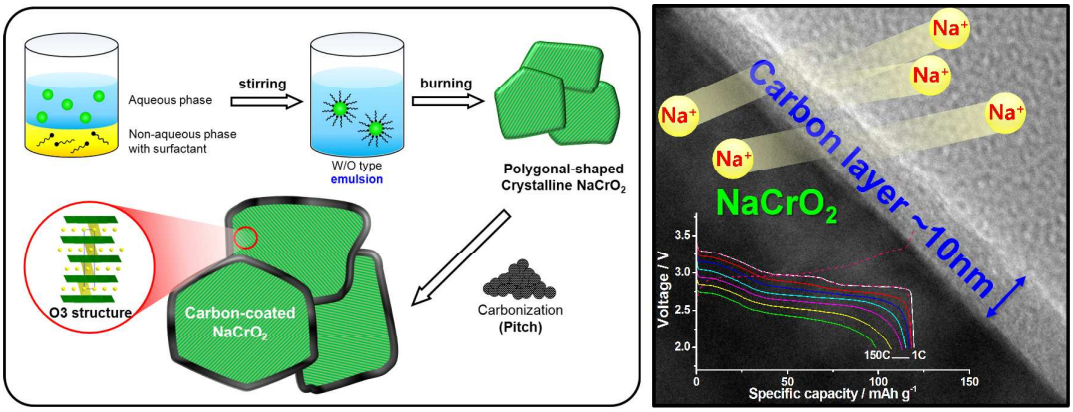

Carbon-coated $NaCrO_2$ synthesized via emulsion method, exhibits excellent cyclability, ultrafast rate capability up to 150 C-rate, demonstrating ideal properties for advanced sodium-ion batteries.

Energy & Environmental Science Accepted Manuscript